A Study of Joint Fixativity in a Joined-Wing Aircraft

Jack O'Banion, Jitai Jhou, Ronald Stearman
Center for Aeronautical Research
The University of Texas at Austin
and
Stephen Smith
Advanced Aerodynamics Concepts Branch
NASA-AMES Research Center
Moffett Field, CA

ABSTRACT

The present study was initiated to compare the stress distributions in a joined-wing structure that result from employing seven different wing-joint fixativities. The joint fixativity refers to the type of attachment that connects the leading-edge tip of the rear wing to the outboard portion of the forward wing trailing edge. The analysis determines the best wing-joint fixativity of a statically loaded idealized joined-wing configuration. That is, the stress distributions resulting from the different wing joints are compared and the "least stressed" condition is taken as the optimum joint configuration. A NASTRAN finite element elastic axis beam type model of a simplified joined-wing configuration is analyzed for a specified nonaeroelastic wing load distribution. Analysis of the wing joint fixativity data produced the following results:

1) wing joints employing unconstrained rotations about the X or spanwise axis produced the lowest wing-stress conditions.
2) wing joints employing unconstrained rotations about the Z or vertical axis produced the highest wing-stress conditions; and
3) varying rotation constraints about the Y or fuselage axis produced little change in the wing-stress distribution.

Appreciation is expressed to Robert W. Bailey, and Adam Abdulrahman, for their effort in carrying out the present study in coordination with a senior engineering design project. Finally, appreciation is also expressed to Julian Wolkovitch, President of ACA Industries, for his helpful discussions.

These theoretical findings are in agreement with experimental studies conducted on an idealized joined wing model.

1.0 INTRODUCTION

The joined wing study described by this paper was the result of a NASA Ames Research Center / University of Texas project initiated in the Summer of 1986 to compare both computed and measured stress distributions in an idealized joined wing structure for seven wing-joint fixativities. The joined wing project efforts were divided into two groups: the Experimental Modeling group and the Finite Element Analysis (FEA) group. The model group was responsible for the design, construction, and testing of the aluminum torque box model presented in Figure 1.1. This model is a highly simplified version of NASA's current JW-1 joined wing aircraft wing configuration. The results of this experiment study are presented in Volume II of this final report [1]. The FEA group was responsible for constructing and testing a mathematical finite element model of the wing configuration designed by the Model group. The results of the finite element analysis study are presented in volume I of this final report [2].

1.1 OBJECTIVE

The objective of the FEA group was to determine the best wing joint fixativity (best combination of forces and moments transmitted between the forward and aft wings) of a statically-loaded-joined-wing producing the "least-stressed" wing configuration. The stress analysis was conducted for the seven wing joint

fixativities presented in Figure 1.2; straight arrows indicate forces transmitted through the wing joint; elliptical arrows indicate moments transmitted through the wing joint. Because of the simplicity of the torque box and elastic axis beam type models used for the stress/strain analysis, only general stress trends will be anaylzed. These trends will be determined as a function of the beam span as opposed to a plane stress or shear flow analysis which would also estimate the stresses around the torque box. Finally, as a first approximation only a linear analysis has been conducted. Beam-column effects leading to geometric stiffness elements have not been included.

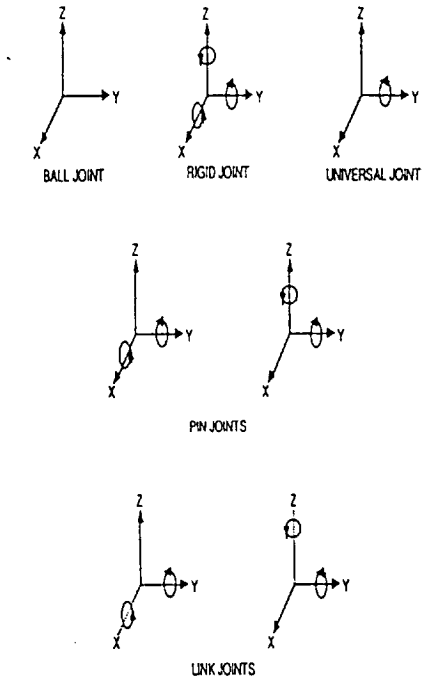

Figure 1.2 - Joint fixativities for joined wing analysis

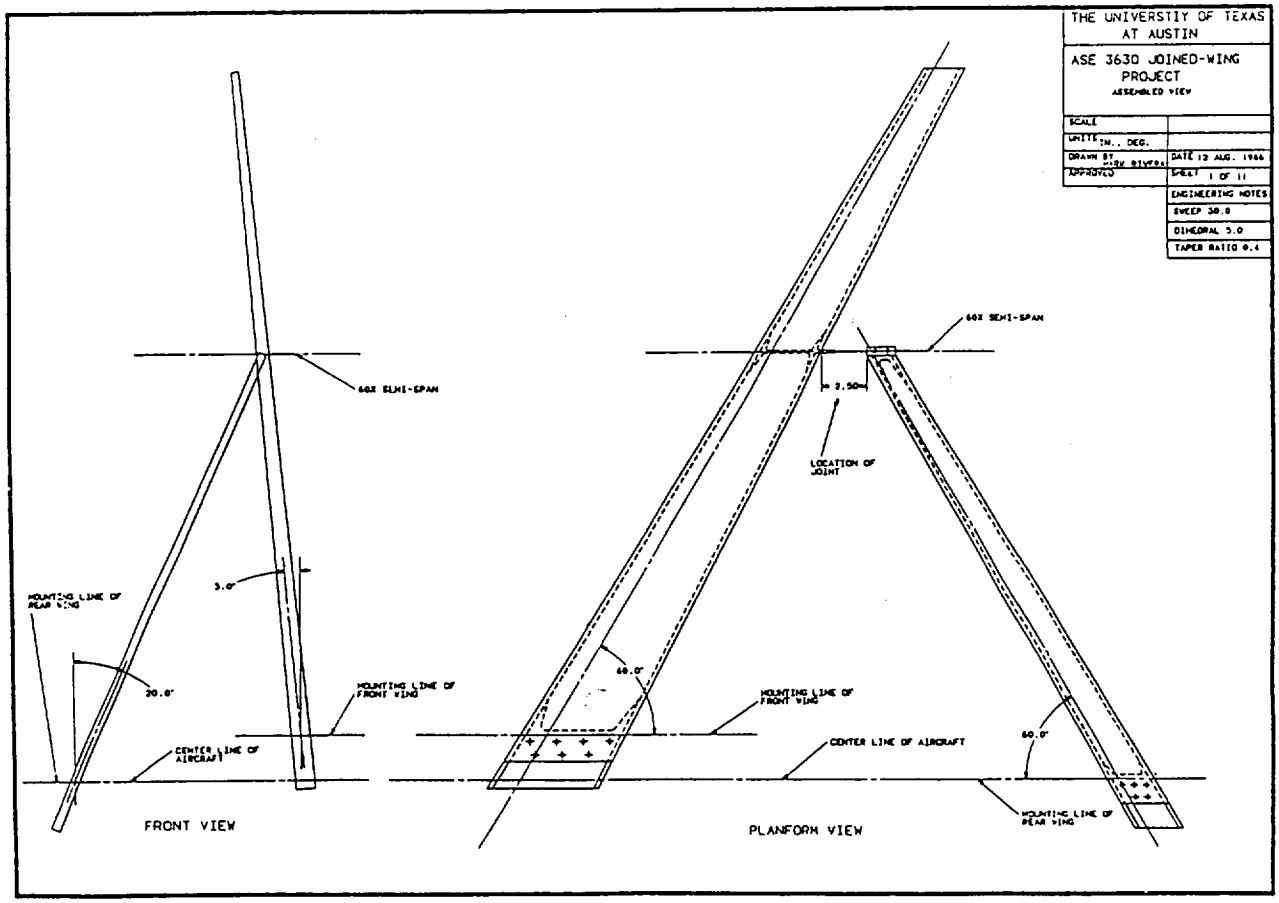

Figure 1.1 - current joined wing configuration

2.0 FINITE ELEMENT MODEL DESCRIPTION

The NASTRAN software package[3] was used for this joined wing finite element analysis. Basically, a NASTRAN model consists of any number of structural elements connected by a common control point grid. This section will describe the NASTRAN finite elements which are applicable to a joined wing torque box model (Section 2.1), the final NASTRAN model used for finite element analysis (Section 2.2), and the methods used to determine the joined wings' cross sectional area and area moments of inertia (Section 2.3).

2.1 NASTRAN FINITE ELEMENTS

Several different NASTRAN elements could be used to model an aircraft wing: CSHEAR, QUAD4, CBAR, and CBEAM. Sections 2.1.1 through 2.1.4 describe these four NASTRAN finite elements.

2.1.1 CSHEAR

The CSHEAR element is a uniform quadrilateral element defined by four coplanar grid points. The CSHEAR element is designed to simulate a thin reinforced skin -- such as the aluminum skin of an aircraft wing. CSHEAR elements are basically membrane elements which are not designed to withstand bending forces and must be used with other finite elements (modeling ribs and spars) which can supply the bending stiffness necessary to create a valid mathematical wing model.

2.1.2 QUAD4

Like the CSHEAR, the QUAD4 is a quadrilateral element, but unlike the CSHEAR, the QUAD4 may be defined by four non-planar grid points and may have a varying thickness. The QUAD4 element is also designed to simulate a thin skin, but the QUAD4 possesses bending stiffness as well as axial and transverse shear stiffness.

For the torque box application described by this report, the QUAD4 element will supply all the bending and shearing resistance necessary for a realistic mathematical model. The CSHEAR element applies more to an actual wing model where ribs and spars are also modeled -- the CSHEAR is not adequate for the torque box application described in this report.

2.1.3 CBAR

The CBAR element simulates a simple uniform bar and is defined by two grid points and several bar cross section properties. A CBAR element provides resistance to torsional and bending moments as well as axial and transverse shear forces. A simple wing of uniform cross section could be lumped as a single CBAR element.

2.1.4 CBEAM

The CBEAM element is exactly the same as the CBAR element except the CBEAM element simulates a bar with a non-uniform cross section. In addition, internal stresses along the length of both the CBAR and CBEAM elements may be extracted from up to nine interior locations in the elements.

Because the joined wing configuration anaylzed for this report is non-uniform (high aspect ratio,taper,dihedral and sweep angle), the CBEAM element provides a more realistic wing model as apposed to a CBAR (or group of CBARs) element.

2.2 FINAL NASTRAN MODEL CONFIGURATION

Both QUAD4 and CBEAM elements were considered for the joined wing finite element model. CBEAM was chosen as the primary element for the joined wing model because of the enormous gain in simplicity over a QUAD4 model. Figure 2.1 presents a QUAD4 version of the joined wing model; Figure 2.2 presents the analogous CBEAM version.

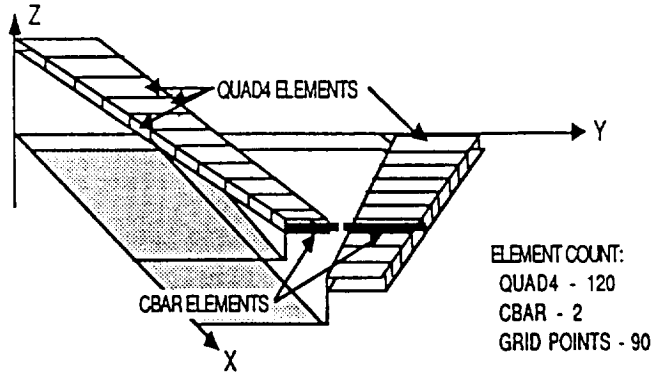

Figure 2.1 - QUAD4 version of joined wing finite element model

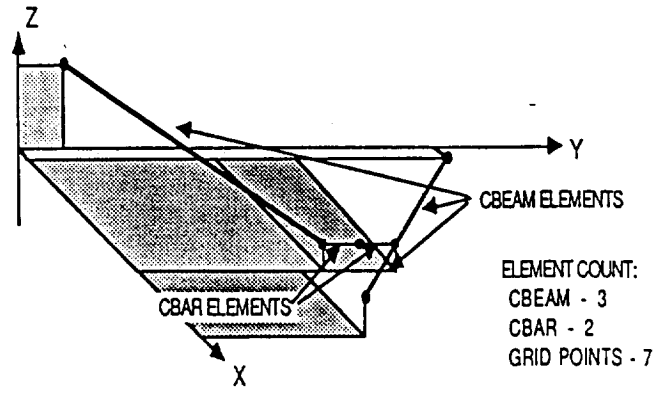

Figure 2.2 - Final joined wing finite element model

The global coordinate system used for joined wing static analysis is defined in Figures 2.1 and 2.2. The QUAD4 version of the joined wing configuration contains 122 elements, but an analogous CBEAM version of the joined wing configuration, with the same output capabilities, requires only five elements -- the difference in computer analysis costs between the two versions is even greater.

Because of the symmetric nature of the torque box model, the elastic axis and geometric centers of the wing models coincide; for this reason, CBEAM grid points were placed along the geometric center of the wing cross sections. The forward wing was modeled using two CBEAM elements (connected at the wing joint); the aft wing with one CBEAM element. CBAR elements were used to model the joint receivers for each wing. Forces and moments are transmitted through the joint (a single grid point) by equating the respective translations and rotations of the joint receivers at the joint.

2.3 WING CROSS SECTION PROPERTIES

NASTRAN CBEAM and CBAR elements require cross sectional properties as program inputs. This section will detail the methods used to calculate the wing cross sectional area, A, the area moments of inertia, I_{yy} and I_{zz}, and the polar moment of inertia, J, which are defined by the wing cross section geometry presented in Figure 2.3. Note: for a symmetric cross section, $I_{yz} = 0$. Based upon the findings of Reference 6 this is not the optimal torque box cross section for a joined wing. It was assumed adequate, however, for the present study.

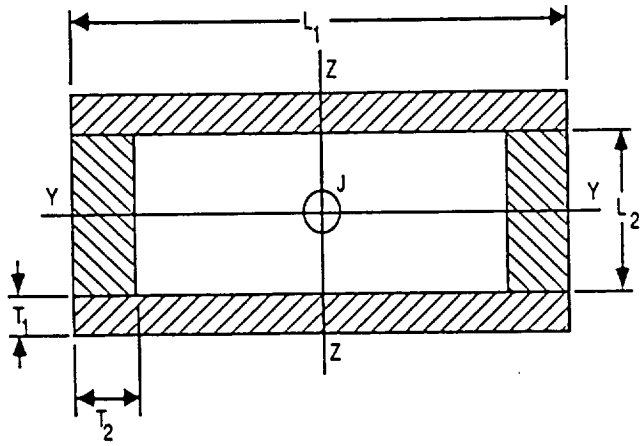

Figure 2.3 - Torque box cross section geometry

2.3.1 AREA/MOMENT OF INERTIA CALCULATIONS

Using the geometric definitions of Figure 2.3 and the basic area moment of inertia integrals, equations (1) and (2)[4], equations (3), (4), (5) and (6) were derived to calculate A, I_{yy}, I_{zz} and J, respectively.

$$I_{yy} = \int z^2\, dA \qquad (1)$$

$$I_{zz} = \int y^2\, dA \quad \text{Where } dA=dydz \qquad (2)$$

$$A = 2(T_1L_1 + T_2L_2) \qquad (3)$$

$$I_{yy} = 0.667L_1((L_2/2 + T_1)^3 - (L_2/2)^3) + T_2L_2^3/6 \qquad (4)$$

$$I_{zz} = 0.667L_2((L_1/2)^3 - (L_1/2 - T_2)^3) + T_1L_1^3/6 \qquad (5)$$

$$J = I_{yy} + I_{zz} \qquad (6)$$

Since the wing cross sections are perpendicular to the joined wings' elastic axis, the root and tip of the swept wings create special modeling problems. However, for slender swept wings with high aspect ratios and applied loads through the wing elastic axis, an effective wing root and tip may be assumed[5], simplifying the wing finite element model. Figure 2.4 presents the effective root and effective tip concepts.

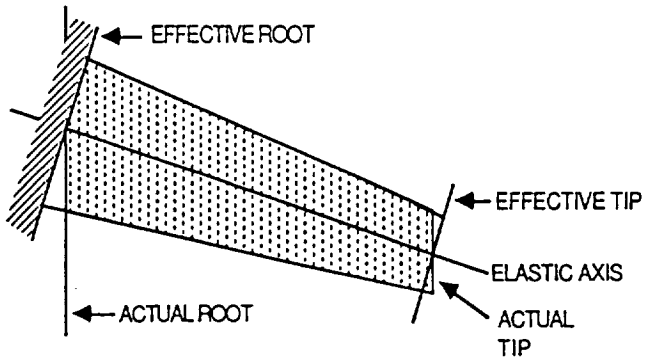

equations (3) - (6) is located in Table 2.1. The corner points of the wing cross sections were also necessary for NASTRAN normal stress outputs. The corner point coordinates, presented in Table 2.2, were calculated at several distances along the wing using simple linear interpolation.

Table 2.1 - Joined wing cross section properties

GRID POINT	L1 (in)	L2 (in)	A (sq in)	Iyy (in**4)	Izz (in**4)	J (in**4)
1	5.154	0.936	0.2248	0.04175	0.6157	0.6574
2	3.362	0.597	0.1458	0.01124	0.167	0.1722
3	1.98	0.336	0.0849	0.00217	0.0411	0.0433
4	2.515	0.436	0.1084	0.00455	0.0854	0.09
5	1.477	0.336	0.0688	0.00167	0.0198	0.0215

T1 = 0.016 in T2 = 0.032 in

CBEAM ELEMENT	DISTANCE FROM ROOT (in.)	NORMALIZED BEAM DISTANCE	Y(in)	Z(in)
1	0.0	0.0	2.577	0.50
1	2.91	0.118	2.471	0.48
1	5.81	0.236	2.365	0.46
1	8.71	0.354	2.260	0.44
1	11.6	0.472	2.154	0.42
1	14.5	0.590	2.048	0.40
1	17.4	0.708	1.942	0.38
1	20.3	0.826	1.837	0.36
1	23.3	0.944	1.731	0.34
0.5	24.56	1.0/0.0	1.681	0.3305
2	26.1	0.081	1.625	0.32
2	29.0	0.234	1.519	0.30
2	31.9	0.387	1.413	0.28
2	34.8	0.540	1.308	0.26
2	37.7	0.693	1.202	0.24
2	40.6	0.846	1.096	0.22
2	43.4	1.0	1.0	0.20
3	0.0	0.0	1.258	0.25
3	1.85	0.062	1.225	0.247
3	3.68	0.124	1.193	0.244
3	5.53	0.186	1.161	0.241
3	9.83	0.331	1.086	0.233
3	17.21	0.579	0.957	0.221
3	22.08	0.745	0.871	0.213
3	25.81	0.869	0.807	0.207
3	27.64	0.931	0.774	0.203
3	28.88	0.972	0.753	0.201
3	29.71	1.0	0.74	0.20

Table 2.2 - Joined wing cross section corner point coordinates

2.3.2 MATERIAL PROPERTIES

The material properties used for all the joined wing finite elements are those of aluminum:
modulus of elasticity, E = 10.6E6 psi,
modulus of rigidity, G = 4.0E6 psi,
and
density, rho = 0.0975 lb/in^3.

3.0 WING LOADING CONDITIONS

This section will describe the loading conditions placed on the joined wing configuration to produce stress distributions through the wings. Section 3.1 will describe joined wing load distributions and Section 3.2 will describe the NASTRAN implementation of the joined wing load distributions.

3.1 LOAD DISTRIBUTIONS

From wing root to wing tip, the load distribution function approximates a sinusoidal shape as seen in Figure 3.1. The sinusoidal shape is based on preliminary vortex-lattice analysis of joined wing load distributions conducted at the NASA / Ames Research Center. The vortex-lattice analysis revealed that the preliminary load distributions could be approximated by a simple cosine function.

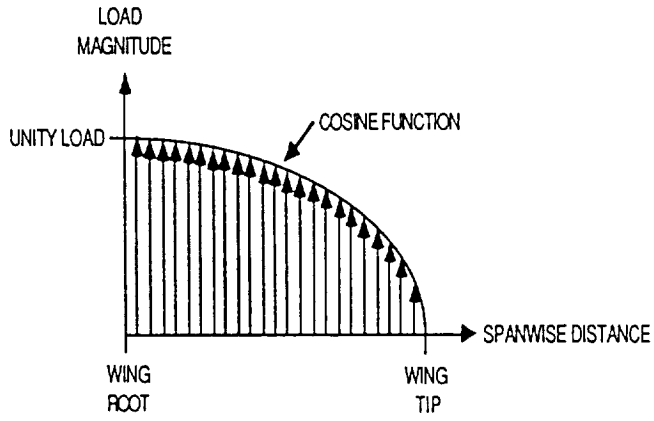

Figure 3.1 - Joined wing sinusoidal load distribution

In a final design analysis other loading conditions should also be examined which include various possible combinations of control deflections and gust loadings. In this preliminary analysis, however, the computational effort was simplified by considering the more standard nonmaneuvering air load distribution. In the assumed load distributions for both forward and aft wings, 90% of the total load was applied to the forward wing and 10% of the total load was applied to the aft wing; the initial total load was set at 100 lbs. to facilitate accurate strain readings in the experimental study. To further facilitate correlations with experimental data the actual spanwise loading distributions was assumed to be a dead weight loading applied parallel to the gravity vector and not normal to the wing plane.

3.2 NASTRAN IMPLEMENTATION

NASTRAN has the capability of applying linearly tapered distributed loads or concentrated loads to a CBEAM element, but not a sinusoidal distributed load. Therefore, the sinusoidal distribution was lumped across five inch spanwise wing segments to produce the desired load distribution. Figure 3.2 illustrates the lumping procedure.

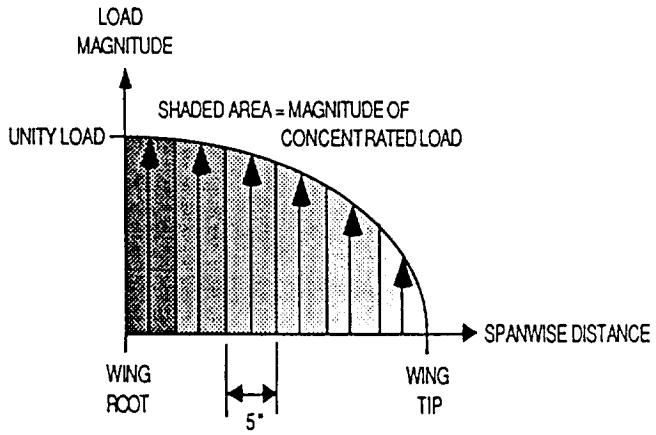

Figure 3.2 - Lumped loads from sinusoidal distribution

Table 3.1 presents the methodology for determining the lumped loads along the elastic axis of the forward and aft wings. The procedure for calculating the loading was as follows:

1) normalize the distance to the applied load from the wing root;
2) multiply normalized distance by $\pi/2$;
3) repeat (2) for a distance of (1) -
4) repeat (2) for a distance of (1) + 2.5 inches -- HIGH;
5) integrate cosine function from LOW to HIGH by subtracting sin(LOW) from sin(HIGH).
6) multiply result of (5) by .9 (90% forward wing) or .1 (10% aft wing); and
7) neglect distance offsets due to torque equalization.

Table 3.1 - Concentrated load calculations for forward and aft wings
FORWARD WING

DISTANCE FROM ROOT (in)	NORMALIZED DISTANCE per CBEAM	NORMALIZED DISTANCE per WING	LOW	HIGH	sin(HIGH)	sin(HIGH) - sin(LOW)	90%
2.5	0.1029	0.0581	0.0		0.1815	0.1815	0.1635
7.5	0.3088	0.1743	0.1825		0.357	0.1755	0.158
12.5	0.5146	0.2905	0.3651		0.5206	0.1636	0.1472
17.5	0.7205	0.4067	0.6041		0.6669	0.1463	0.1317
22.5	0.9263	0.5229	0.7301	0.581	0.7911	0.1242	0.1118
27.5	0.1713	0.6391	0.9126		0.889	0.0979	0.0881
32.5	0.4381	0.7553	1.0952		0.9573	0.0683	0.0615
37.5	0.7049	0.8715	1.2777		0.9939	0.0366	0.0329
41.5	0.9184	0.9649	1.4602	1.5708	1.0	0.0061	0.0055

Table 3.1 (cont.) - Concentrated load calculations for forward and aft wings
AFT WING

DISTANCE FROM ROOT (in)	NORMALIZED DISTANCE	LOW	HIGH	sin(HIGH)	sin(HIGH) - sin(LOW)	10%
2.5	0.0842	0.0		0.2616	0.2616	0.0262
7.5	0.2527	0.2647		0.5048	0.2432	0.0243
12.5	0.4212	0.5292		0.7131	0.2083	0.0208
17.5	0.5896	0.7939		0.8716	0.1585	0.0159
22.5	0.7581	1.0018		0.9695	0.0979	0.0098
27.34	0.9212	1.3231	1.5708	1.0	0.0305	0.0031

4.0 RESULTS

NASTRAN static analysis simulations were performed on the joined wing model defined in Section 2.0 using the load distribution discussed in Section 3.0 for each of the seven wing joint fixativities presented in Section 1.0. This section will present a comparative analysis of the wing stress resultants, i.e., forces and moments (Section 4.1), the best wing joint fixativity based on the comparative analysis or a least stressed configuration (Section 4.2), and a wing deformation analysis based on the best wing joint fixativity (Section 4.3).

4.1 COMPARATIVE ANALYSIS

NASTRAN provides the following output parameters for both ends of a CBEAM element and at up to nine interior cross sections of the CBEAM element:

1) maximum axial stresses,
2) bending moments (two planes),
3) torsional moments (along elastic axis),
4) shear forces (two planes),
5) axial forces, and
6) axial stresses at four points on the beam cross section (set as torque box corner points for this study).

Figure 4.1 shows the CBEAM cross sectional geometry and defines the output parameters. Translations and rotations of the wing joint are defined in the global coordinate system presented in Figures 2.1 and 2.2.

Figure 4.2 presents the maximum axial stress along the spanwise length of the forward wing for all seven joint fixativities (Figures 4.2 through 4.10 are located at the end of this section). These stresses represent the maximum absolute value of the stresses among the four cross section corner points and include stress contributions from axial forces and bending moments. One joint clearly provides a better (lower) axial stress

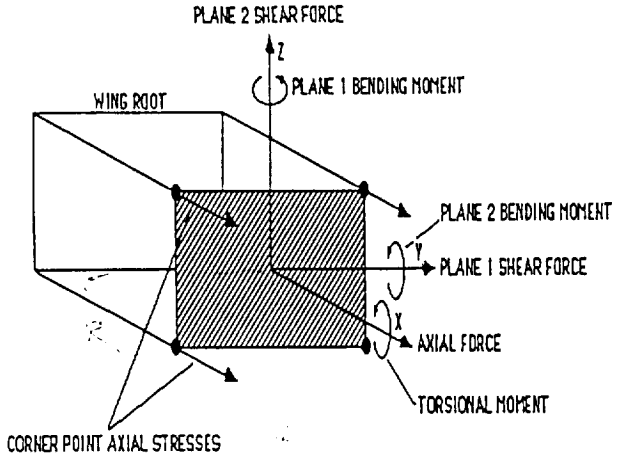

Figure 4.1 - CBEAM output parameter definitions

distribution than the other: the link joint with unconstrained Z translations and X rotations (ZTXR). Conversely, data analysis reveals the worst joint fixativity (highest stresses) as the link joint with unconstrained X translations and Z rotations (XTZR). Other results from Figure 4.2 include the following observations.

1) Starting with the best joint fixativity (link ZTXR), constraining the Z translations produced the next best joint fixativity (pin XR), and then constraining all rotations (fixed joint) comes close to producing the third best joint fixativity.
2) Joint fixativities with unconstrained Z rotations produced the two worst axial stress distributions (link XTZR, pin ZR).
3) Constrained and unconstrained Y rotations produce seemingly identical stress curves (i.e., universal joint compared to ball joint).

The discontinuities in the stress curves at about 24" of spanwise length mark the location of the wing joint on the forward wing; for the aft wing, the joint is located at the wing tip -- no discontinuities. Figure 4.3 presents the maximum axial stresses for the aft wing. The trends observed in Figure 4.2 also apply to Figure 4.3, but analyzing the figures together reveals the following information.

1) When comparing the pin ZR and link XTZR joints, constraining the X translation has the affect of increasing the maximum axial stress levels near the aft wing tip.
2) Between the ball and universal joints, constraining the Y rotations produced larger axial stresses especially near the aft wing tip.
3) Joints allowing Z rotation generally increase axial stress levels in the rear wing at the joint.

Figures 4.4 and 4.5 are normalized (with respect to the maximum stress at the wing root) representations of Figures 4.2 and 4.3 respectively. Figures 4.4 and 4.5 suggest the best joint fixativities, in terms of maximum axial stress, also produce the most rapid decrease in stress levels through the wings. Again it is evident, however, that wing joints with unconstrained Z and X rotations produce the highest stress at the tip of the rear wing.

Figures 4.6a and 4.6b present the Plane 1 bending moments along the forward and aft wings respectively. The most important aspect of these two sets of curves is that vertical loads on the joined wing configuration produce horizontal or chordwise bending moments in both wings. This result is due to the swept-dihedral joined wing configuration. A vertical force applied in the global coordinate system has three separate components when applied in a wing local coordinate system. In terms of best-to-worst joint fixativities, Figures 4.6a and 4.6b agree with the previous results from Figures 4.2 through 4.5, but notice the forward wing Plane 1 bending moments are consistently about four times greater than the aft wing Plane 1 bending moments. The forward wing takes more of the Plane 1 load because 90% of the total load is applied to the forward wing -- the aft wing takes aproximately 20% of the Plane 1 load because of its higher dihedral angle (about 30 degrees).

Figure 4.7 presents the Plane 2 bending moments for the forward and aft wings. An order of magnitude separates the Plane 2 moments from the Plane 1 moments; another order of magnitude separates the forward wing Plane 2 moments from the aft wing Plane 2 moments. These results are roughly consistent with the 90%/10% forward/aft load distribution. Distinguishing optimum joint fixativities is difficult for these sets of curves, but best-to-worst joint fixativities agree with previous figures (other stresses) for the aft wing. However, as the Plane 2 moments increase on the aft wing, ZTXR appears as the best fixativity while on the forward wing a reversing of the best-to-worst order for the forward wing joint fixativities occurs. Because the seven curves for the forward wing are so similiar and nearly identical (relative to the aft wing curves), the previous best-to-worst joint fixativity comparisons remain unaltered.

Figures 4.8 presents the forward and aft wing Plane 1 shear forces; Figure 4.9 presents the Plane 2 shear forces for the forward and aft wings. These plots show magnitude differences similiar to the magnitude differences between the Plane 1 and Plane 2 bending moments. The discontinuities appearing through the shear force curves are due to the concentrated load implementation of the assumed distributed load (Section 3.0). Figure 4.10 presents the axial forces through both wings. These small axial forces are due to the vertical loads acting on the dihedral wings.

Table 4.1 lists the torsional moments in each wing for each wing joint fixativity. Since the applied loads were taken at the elastic axis no externally applied torques occur. Torsional moments were thus constant through the inboard (wing root to joint) portion of the forward wing and the entire length of the aft wing; torsional moments were zero for the outboard (joint to wing tip) portion of the forward wing. Torsional moments are caused by the forces transmitted through the wing joint to the ends of the wing joint receivers. The joint receivers act as lever arms for all three local wing axes, including the wing's elastic axis. Since the concentrated loads were applied through the elastic axis of each wing, the moments about the elastic axis of one wing can only be caused by the applied loads on the other wing which are transmitted through the wing joint. Intuitively, the rigid joint would produce the largest torsional moment because all moments and forces must be transmitted through the wing joint -- Table 4.1 shows this intuition to be true.

Table 4.1 - Torsional moments for forward and aft wings

JOINT	TORSION ALONG THE WING AXIS (lb-in)	
	FORWARD (inboard)	AFT
UNIVERSAL	-1.04	-0.45
PIN XR	-1.13	-1.35
BALL	3.37	4.06
LINK ZTXR	-6.04	-6.09
PIN ZR	23.66	-10.5
LINK XTZR	25.71	-11.93
RIGID	26.23	-13.05

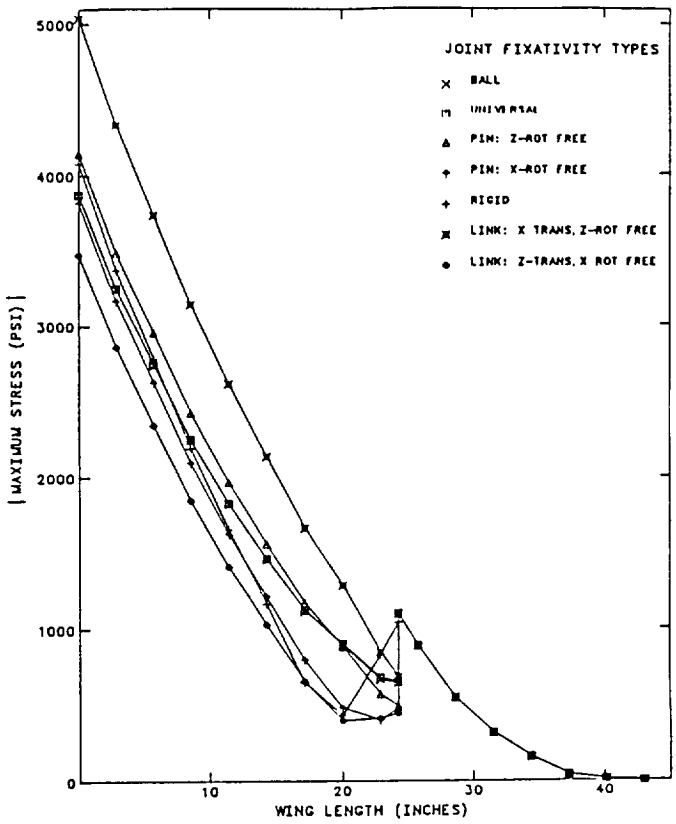

FIGURE 4.2: MAX AXIAL STRESS VERSUS SPANWISE LENGTH-FORWARD WING

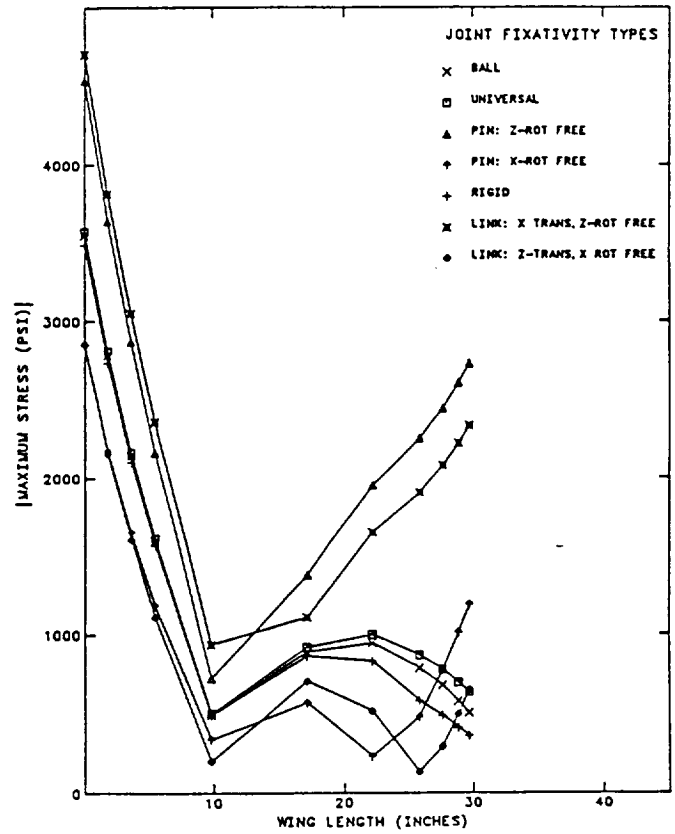

FIGURE 4.3: MAX AXIAL STRESS VS SPANWISE LENGTH-AFT WING

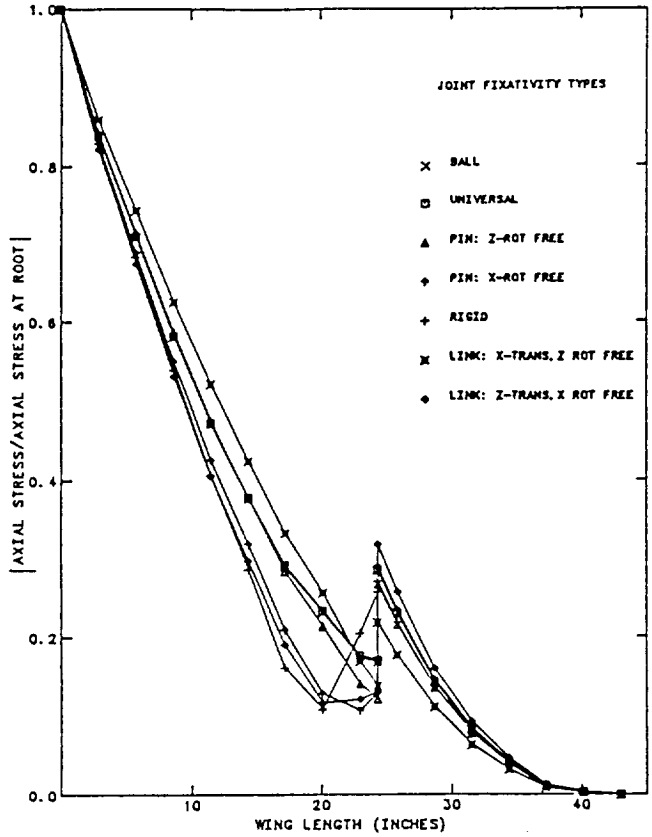

FIGURE 4.4: NORMALIZED SPANWISE MAX STRESS-FORWARD WING

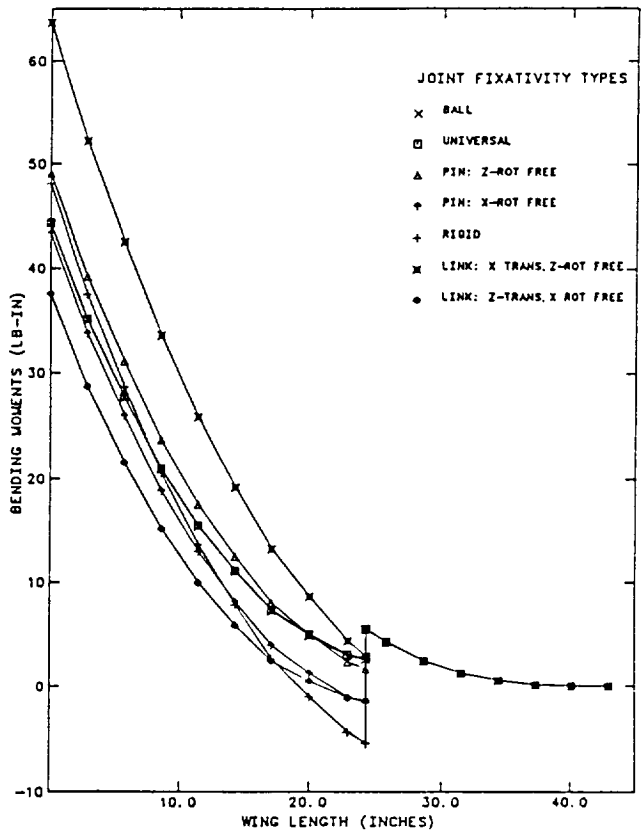

FIGURE 4.6A: PLANE 1 BENDING MOMENTS VS SPANWISE LENGTH-FORWARD WING

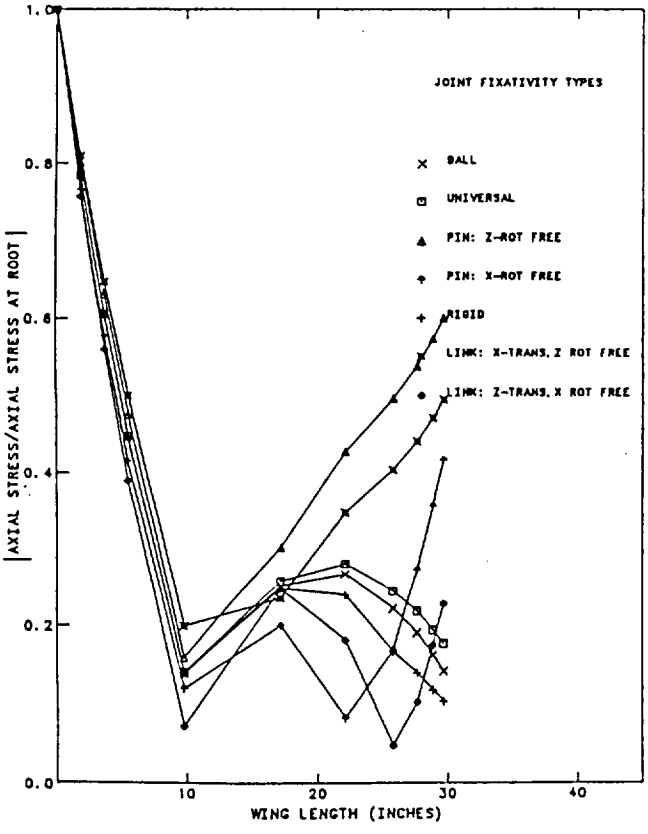

FIGURE 4.5: NORMALIZED SPANWISE MAX AXIAL STRESS-AFT WING

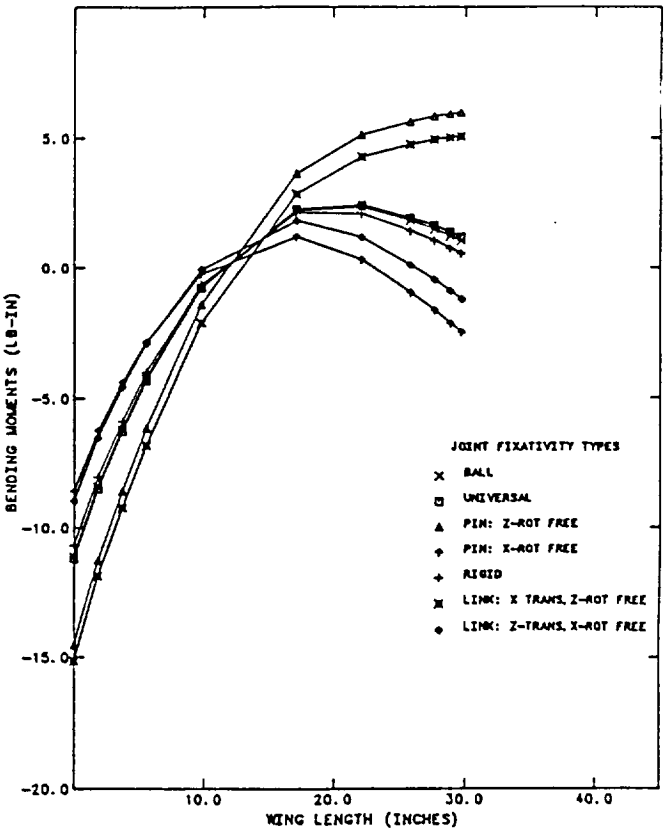

FIGURE 4.6B : PLANE 1 BENDING MOMENTS VS SPANWISE LENGTH-AFT WING

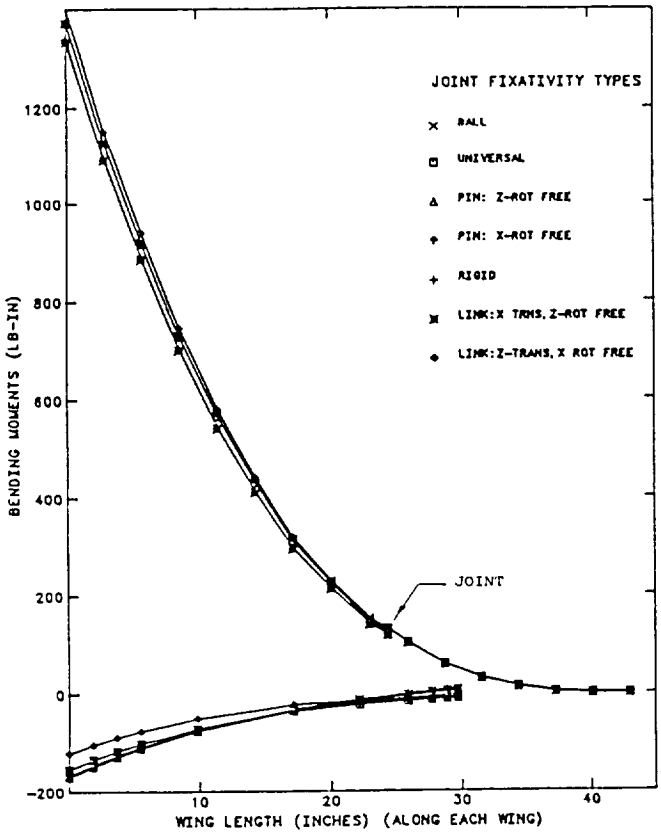

FIGURE 4.7:PLANE 2 BENDING MOMENTS VS SPANWISE LENGTH-BOTH WINGS

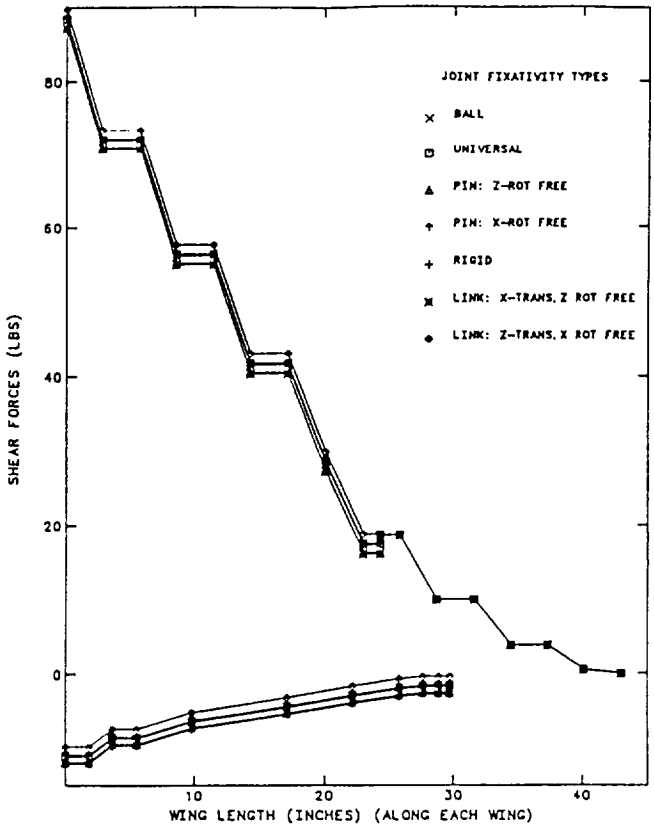

FIGURE 4.9: PLANE 2 SHEAR FORCES VS SPANWISE LENGTH-BOTH WINGS

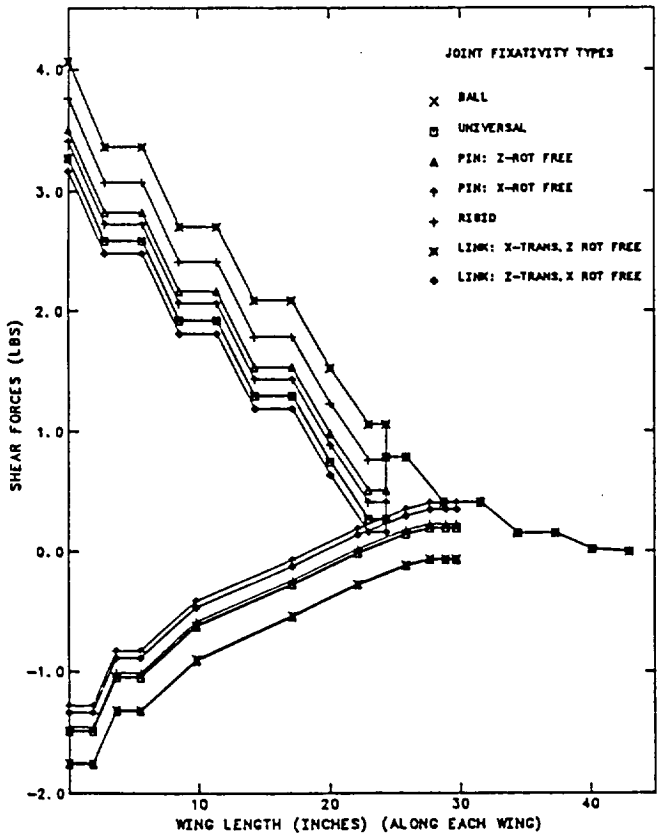

FIGURE 4.8: PLANE 1 SHEAR FORCES VS SPANWISE LENGTH-BOTH WINGS

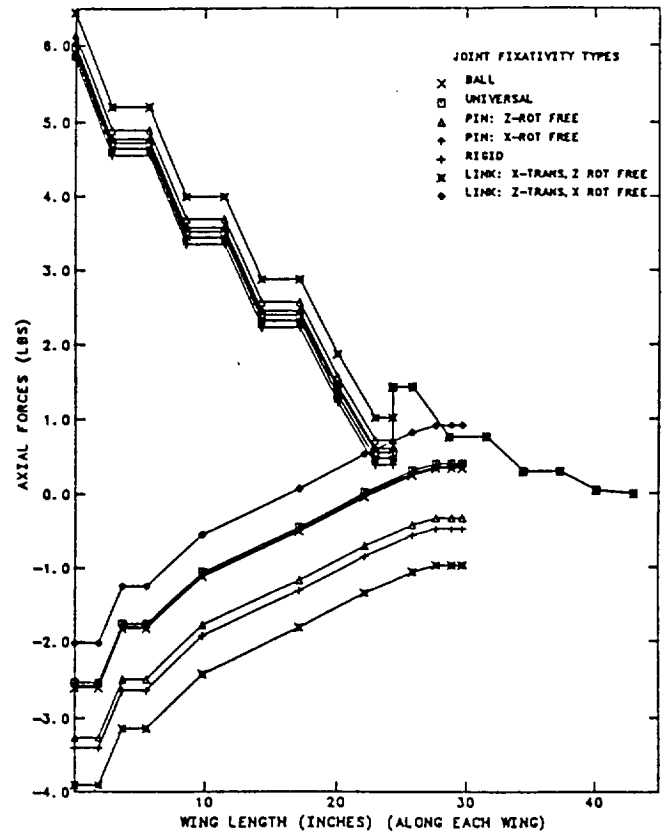

FIGURE 4.10: AXIAL FORCES VS SPANWISE LENGTH-BOTH WINGS

4.2 BEST WING JOINT FIXATIVITY

Each of the Figures 4.2 through 4.10 reveal a best-to-worst order for joined wing joint fixativity; Table 4.2 summarizes these results. Joint fixativities in Table 4.2 are ranked 1 for best fixativity and 7 for worst fixativity in terms of the stress/force/moment distributions through both joined wings. Table 4.2 clearly shows the link joint with unconstrained Z translations and X rotations to be the best of the joint fixativities tested for this report. Note that the link ZTXR joint does not allow Y translations between the wings; i.e., the wings are not able to fold over each other. The link ZTXR joint may be visualized as a pin XR joint mounted to the forward wing which would slide along a vertical guide mounted to the aft wing -- overall, a complex joint. The simpler pin XR joint exhibits slightly degraded performance compared to the link ZTXR joint, but may be worth the performance drop when joint complexity and reliability are considered in the joined wing design process. Finally, other factors such as flutter and divergence (i.e., stiffness effects) must be investigated and compared with the strength studies conducted here to arrive at the most optimal wing joint fixativity for final design considerations.

Table 4.2 - Joint fixativity stress/force/moment distribution summary

STRESS/FORCE/MOMENT \ JOINT	LINK ZTXR	PIN XR	RIGID	BALL	UNIVERSAL	PIN ZR	LINK XTZR
MAXIMUM AXIAL STRESS FORWARD WING	1	2	3	4	4	6	7
MAXIMUM AXIAL STRESS AFT WING	1	2	3	4	5	7	6
PLANE 1 BENDING MOMENTS FORWARD / AFT WINGS	1	2	3	4	4	6	7
PLANE 2 BENDING MOMENTS FORWARD / AFT WINGS	1	2	5	2	2	5	5
PLANE 1 SHEAR FORCES FORWARD / AFT WINGS	1	2	5	3	3	6	7
PLANE 2 SHEAR FORCES FORWARD / AFT WINGS	1	2	5	2	2	5	5
TORSIONAL MOMENTS FORWARD / AFT WINGS	4	1	7	3	1	5	6

4.3 WING DEFORMATIONS

Table 4.3 lists the translation and rotation displacements experienced by each wing's joint receiver at the wing joint. This data confirms the constrained/unconstrained natures of each joint fixativity; displacements are referenced to the global coordinate system.

Table 4.3 - Joined wing joint static displacements

JOINT FIXITY		DISPLACEMENT AT JOINT (in)			ROTATION AT JOINT (rad)		
		X	Y	Z	X	Y	Z
BALL	FORWARD	8.6E-3	1.8E-2	5.3E-2	-1.6E-3	-2.9E-3	1.1E-3
	AFT	SAME	SAME	SAME	1.7E-3	-1.8E-3	-7.7E-4
UNIVERSAL	FORWARD	8.7E-3	1.8E-2	5.3E-2	-1.7E-2	-2.6E-3	1.1E-3
	AFT	SAME	SAME	SAME	1.2E-3	SAME	-6.4E-4
PIN ZR	FORWARD	1.0E-2	2.0E-2	5.0E-2	-9.4E-4	-2.9E-3	1.3E-3
	AFT	SAME	SAME	SAME	SAME	SAME	-1.4E-3
PIN XR	FORWARD	6.5E-3	1.6E-2	5.3E-2	-1.5E-3	-2.6E-3	6.0E-4
	AFT	SAME	SAME	SAME	1.4E-3	SAME	SAME
RIGID	FORWARD	7.1E-3	1.7E-2	4.9E-2	-8.2E-4	-3.0E-3	-4.0E-4
	AFT	SAME	SAME	SAME	SAME	SAME	SAME
LINK XTZR	FORWARD	3.4E-3	2.7E-2	5.0E-2	-9.3E-4	-2.9E-3	-5.5E-4
	AFT	1.7E-2	SAME	SAME	SAME	SAME	2.0E-3
LINK ZTXR	FORWARD	4.3E-3	1.3E-2	5.4E-2	-1.7E-3	-2.5E-3	3.8E-4
	AFT	SAME	SAME	3.4E-2	2.4E-4	SAME	SAME

Figures 4.11 and 4.12 present the stress distributions through the forward and aft wings, respectively, for each of four wing cross section corner points. Figure 4.11 shows that the right side (forward side) of the forward wing goes from a compressive state at the wing root toward a tensile state at the wing joint. These compression/tension characteristics suggest the forward wing statically deforms between the root and joint, in the chordwise plane, into a shape similar to an 's' shape deflecting forward and reversing back at the joint. The tip of the forward wing then goes back into compression forward of the joint suggesting a bend forward in this region. From Figure 4.12, the right side of the aft wing goes from a tensile state at the wing root, to a compressive state at midspan, back to a tensile state at the wing joint. These compression/tension characteristics suggest the aft wing statically deforms, in the chordwise plane, into an 'n' shape that is deflecting aft at both ends.

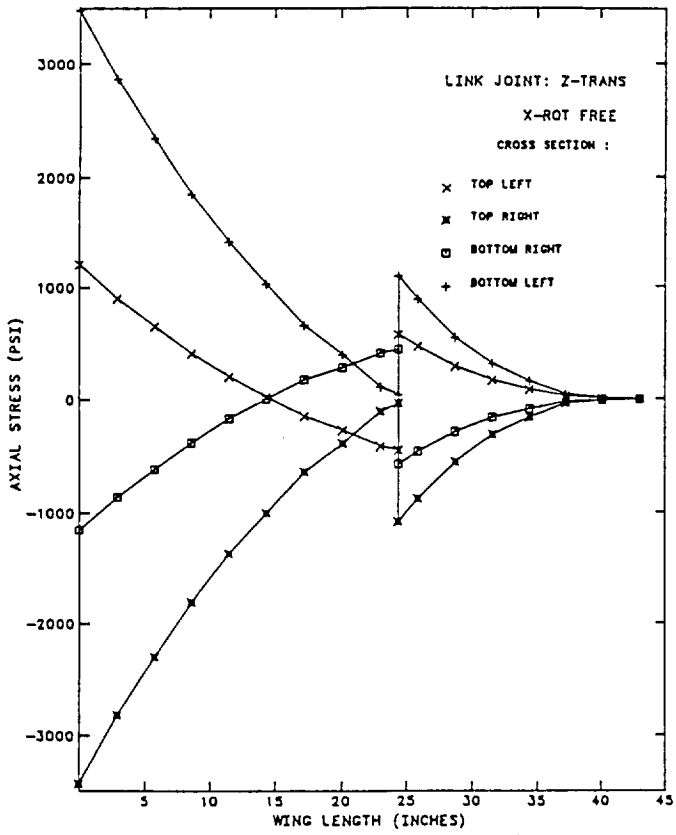

FIGURE 4.11: CROSS SECTION SPANWISE AXIAL STRESS-FORWARD WING

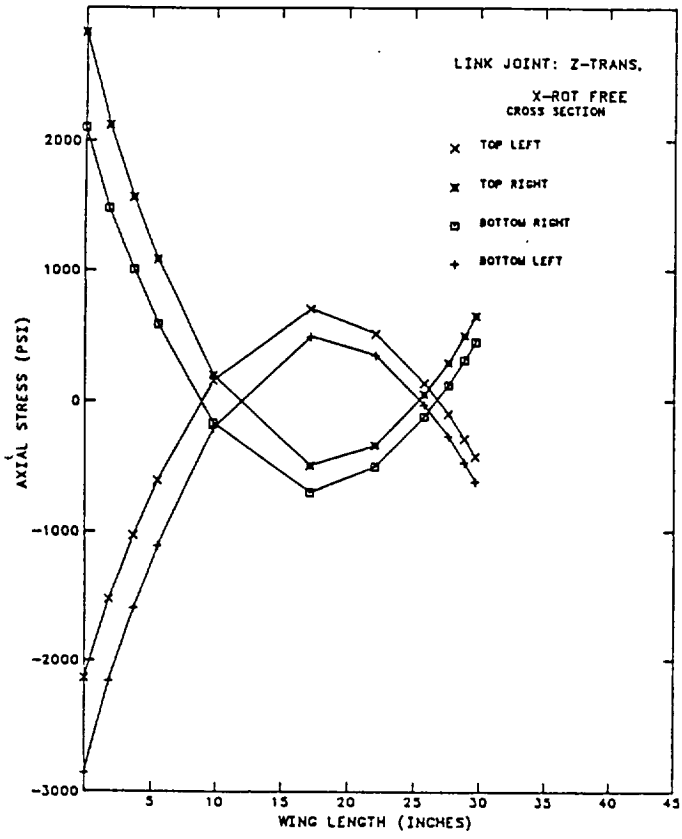

FIGURE 4.12: CROSS SECTION SPANWISE AXIAL STRESS-AFT WING

5.0 CONCLUSIONS

Several important points may be concluded concerning the joined wing joint fixativity anaylsis presented in this report:

1) specifically, unconstrained X rotations and Z translations (link ZTXR) produced the best wing joint fixativity (of the joints examined); generally, the best joint fixativities incorporated unconstrained X rotations (link ZTXR, pin XR); Best joint fixativities imply "least stressed" wing conditions under a specified loading.
2) Y rotation constraints on the joint fixativity do not appreciably effect the stress/force/moment distributions through the joined wings; and
3) in general, the worst joint fixativities incorporate unconstrained Z rotations.

To determine the best wing joint fixativity for a joined wing, "stiffness" as well as "strength" considerations must be considered. That is, flutter and divergence as well as stress distributions must be checked for a given joint configuration.

6.0 REFERENCES

1 O'banion, J. and R. Stearman , *A Study of Joint Fixativity in a Joined-Wing Aircraft, Volume II,* Center for Aeronautical research report, The University of Texas at Austin, March 1987

2 O'banion, J., J. Jhou, and R.Stearman, *A Study of Joint Fixativity in a Joined-Wing Aircraft, Volume I,* Center for Aeronautical research report, The University of Texas at Austin, January 1987

3 *MSC/NASTRAN Handbook for Linear Static Analysis -- MSC/NASTRAN Version 60,* The MacNeal-Schwendler Corporation, June 1980.

4 Beer, F.P. and Johnston, E.R. Jr., *Mechanics of Materials,* McGraw-Hill Book Company, New York, 1981, p. 579.

5 Bisplinghoff, R.L., Ashley, H. and Halfman, R.L., *Aeroelasticity,* Addison-Wessley Publishing Company, Cambridge, Mass, 1955, p. 47.

6 Fairchild, M.P., *Structural Weight Comparison of a Joined Wing and a Conventional Wing,* Journal of Aircraft Vol.19, No.6, June 1982